

Change of Mechanical behavior of a compacted well-graded granular material with and without cement

Devi Prasad Singh, Jyoti Prakash Das, Amlan Pattanayak, Subhankar Shibajyoti Puhon

Department of Civil Engineering, NM Institute of Engineering and Technology, Bhubaneswar, Odisha
Department of Civil Engineering, Raajdhani Engineering College, Bhubaneswar, Odisha
Department of Civil Engineering, Aryan Institute of Engineering and Technology Bhubaneswar, Odisha
Department of Civil Engineering, Capital Engineering College, Bhubaneswar, Odisha

ABSTRACT: Concrete increases improve the presentation of granular soils. Be that as it may, most writing instances of concrete augmentations are in inadequately evaluated sands, either to imitate the conduct of sandstones or to complement the mechanical differences among established and uncemented soils. In this article, the conduct of an all around evaluated granular soil, utilized for base and sub-base of streets, was concentrated by doing triaxial tests on solidified and uncemented tests. Tests were compacted to accomplish a thick texture and tried at stresses ordinarily utilized in practice. Sieving was utilized to comprehend if breakage is significant and to decide the grain size disseminations of the examples after compaction and shearing. The outcomes show that the expansion of little rates of concrete extraordinarily increment stiffness and widening. Along these lines, creating bigger qualities; this is especially significant at low confining stresses in streets and stopping regions, where this material is usually utilized. Everywhere strains, the outcomes show that different Critical State Lines exist for both the uncemented and solidified soils. Each line has a different slant, which is accepted to be the aftereffect of the development of the grain size appropriation of the established soil. The standardized information demonstrate that an extraordinary state limit surface can be resolved for every one of the three tried soils.

Keywords: Cemented soil; Compacted soil; Triaxial test; Critical state; Base and sub base; Granular soil

INTRODUCTION

Research in uncemented granular material has highlighted the importance of breakage, where the onset of breakage in the NCL is a function of the mineralogy of the grains [12]. Breakage is important as it also marks the location of the CSL, and many researchers have shown that by changing the grain size distribution, the CSL will also change (Thevanayagam et al., 2002, Carrera et al., 2011; Xiao et al., 2016). In structured sands, only a few researchers considered the changes in particle size distribution (PSD) and its effect on altering the location of the CSLs and NCLs, when compared to the uncemented samples (Cuccovillo and Coop, 1997a; Marri et al., 2012). Certain results have shown that due to cementation, the resultant CSL would have a reduced gradient (Cuccovillo and Coop, 1997a), whilst others have shown that the cementation increases the gradient of CSL (Schnaid et al., 2001). In the aforementioned research, it is not clear if the alterations of the CSL gradient are due to particle breakage, bond degradation or a combination of both. Different critical state lines for the same samples with different cement contents are also reported by Cruz et al. (2011). The DEM results have shown that alterations in the CSL are due to the breakage of the bonds and the generation of a different grain size distribution, as some of the particles are still cemented together (Yu et al., 2014; Yu et al., 2015). The alteration of the CSL due to breakage was also investigated by Ghafghazi et al. (2014), where they claimed that breakage causes a downward parallel shift in the CSL, and according to Bandini and Coop (2011), large amounts of breakage are needed for significant changes to occur.

In the majority of the research encountered so far, the samples were prepared using poorly graded granular materials (sands of aeolian origin) or with lower densities; this was done in order to accentuate the breakage or the improvement caused by the binding agent added. In a couple of articles (Rios et al., 2014; Consoli et al., 2014) well graded residual soils are reinforced with cement, however some of them have fines and there is no attempt to measure or determine the breakage.

When well graded soils are used the research tends to concentrate on the mechanical properties of the material at small strains i.e. stiffness and strength up to peak, using multiple-step loading triaxial tests (Kongsukprasert and Tatsuoka, 2007 and Taheri et al., 2012). These tests have the advantage of allowing the use of a single sample to cover a large range of stresses, however it is unclear what the effect of damage to the cement bonds and particle breakage is from the previous loading steps. Hence, the effect of the addition of cement on manmade materials used for engineering purposes is not very well understood.

The purpose of this paper is then to study the effect of small levels of cementation on a very dense fabric, created by compaction of a well graded granular material, under monotonic loading, on commonly used soils. The improvement of the mechanical properties and examines the effects of cementation within the Critical State framework is also explored.

1. Material tested

The soil used in this research was a crushed limestone with 88% CaCo₃, collected from a depot in South London and is currently used commercially for the bases of roads in Southern England. The soil was wet sieved and each particle size range was stored in separate bags. The main properties of this material are summarised in Table 1, with the particle size distribution (PSD) shown in Fig. 1, together with the range defined by the UK Highways Agency (2016) for a base and sub-base type.

The idealised grading curve proposed by Fuller and Thompson (1907) is based on the idea that when larger particles are in contact with each other, larger voids are generated and occupied by intermediate particles; this procedure is then followed to the smallest size available. The idealised curve generates dense fabrics and was then used to correct the initial grading curve of the soil, given that the particles are not spherical, it is argued that it then does not generate the densest possible fabric. Given the sizes of the particles available, the PSD named ‘‘Adjusted grading’’ (Fig. 1) was used for all the tests. This curve follows the Fuller curve for the largest sizes, and below the size 3.35 mm it was translated downwards as not enough material was available. For the same reason, sizes below 0.425 were chosen to make sure that all samples would have the same grain size distribution and the grading within the Type 1, as defined by the UK Highway Agency (2016) for a base and sub-base. As the triaxial equipment used is capable to test samples up to 100 mm diameter and 200 mm high, the grain size distribution was truncated at 20mm.

Cemented samples were created by adding Portland cement classified as CEM1, in accordance to the British Standards (BSEN 1197-1:2011). Given the high strength of the compacted samples, only small percentages of cement (1 and 2%) were used to generate modest changes in strength that could be tested in triaxial equipment.

2. Apparatus and sample preparation

A computer-controlled triaxial apparatus, with a local strain measurement system capable of measuring 10⁻⁶ strain, similar to Cuccovillo and Coop (1997b), was used for the conventional triaxial tests (Fig. 2). The system uses RDP electronics LVDTs (model D6/05000) attached to a modulator/demodulator (model S7DC) that allow the full configuration of the output electric signal. At the beginning of the shearing, the local instruments are reset to zero to take advantage of the 16-bit auto scale of the data logger. The volumetric strain was measured using the volume gauge and the local instrumentation. The desired amount of each fraction of soil was thoroughly mixed in a tray, with different moisture contents, before being compacted in 5 layers, using 27 blows of a 5 kg hammer falling from a height of 450 mm (BS1377-4, 1990). A compaction curve for the uncemented soil was determined in order to define the optimum moisture

Table 1
The index properties of research material from dry sieving.

Description	Crushed limestone
Max density-vibrating hammer (g/cm ³)	2.24
Max void ratio	0.83
Min density (g/cm ³)	1.51
Min void ratio	0.23
Particle density (g/cm ³)	2.76
Max dry density-automatic heavy compaction (g/cm ³)	2.24
Optimum water content (modified proctor)	6%
Type of soil	GW
D ₁₀ (mm)	0.2
D ₃₀ (mm)	1.5
D ₅₀ (mm)	3
D ₆₀ (mm)	4
Uniformity coefficient $C_u = \frac{D_{60}}{D_{10}}$	20
Curvature coefficient $C_c = \frac{D_{30}^2}{D_{10} D_{60}}$	4.8

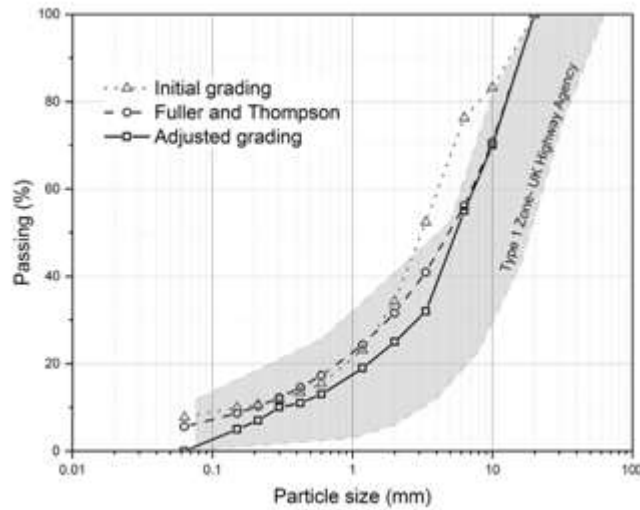


Fig. 1. Particle size distributions: Initial grading; Fuller and Thompson(1907)andtheAdjustedgrading. Thegreybanddefinestherangeoftype 1 (UK Highway Agency,2016).

content. Given that the cemented and uncemented samples were tested, a decision was made to compact all samples with a moisture content of around 10%, providing enough water for cement hydration at the cost of a lower dry density. Table 2 contains the properties of every sample tested. After compaction, the uncemented samples were transported to the pedestal of the triaxial equipment for testing. Suction maintained that the sample was intact before the confining pressure was applied and the percolation procedure started.

The cemented samples were prepared with two different percentages of cement (45 g for 1% and 90 g for 2% cement); where an equivalent mass was removed from the smallest grading of the samples' PSD. The sample preparation followed a similar procedure to the one described above, except that the cement and dry soil were thoroughly

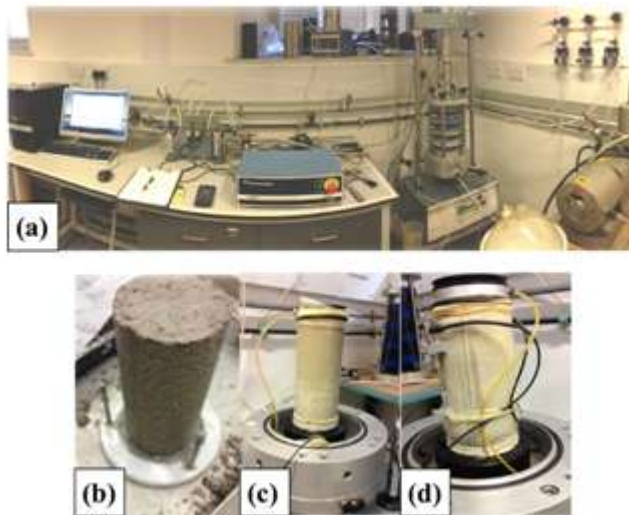


Fig. 2. Picture of the equipment and samples: (a) triaxial equipment in the lab; (b) compacted sample in the pedestal and sample with local instrumentation before closing the triaxial chamber.

mixed together before adding the same water amount, mixing was then continued until homogeneity was achieved. After compaction the sample and mould were put inside of a plastic bag and allowed to cure for 24 h. The sample was then placed inside of a tank with water at 22°C and allowed to cure, submerged, for another 4 days. At day 5 the sample was removed from the tank, mounted on the tri-axial pedestal and prepared for testing. This

procedure was followed to guarantee that the cement could hydrate fully. A volume in excess of 2000 cc of water was percolated through the sample to remove air bubbles. The pressure applied was around 18 kPa, caused by the difference in height between a water container located approximately 2 m above the sample and the outlet from the pedestal. The water coming from the sample was clear and the authors believe that no cement particles were removed from the sample during percolation. The sample was then saturated, maintaining an effective stress of 15 kPa. A B-parameter test was performed at different back pressures, from 100 to 350 kPa on the first sample. Whilst it increased slightly up to 250 kPa, the increase at 300 and 350 kPa were negligible (values measured were of the order of 0.86 to 0.92). It is important to mention that the volume gauge only changed slightly during the increase in pressures, being fairly constant once the required pressures were maintained. This indicated that the sample was saturated and the B-parameters would not reach the required value. Therefore, a minimum back pressure of 250 kPa was used in all drained tests and monitored by another transducer at the top of the sample.

In the consolidation stage the effective stress was raised to the value used in the test. This procedure would take around 2 to 3 days before shearing; however, the cemented samples were all sheared in a drained way at the end of day

Table 2

Properties of the samples tested: the name indicates the cement percentage and the confining stress used during shearing.

Test Name	W_0 (%)	* e_0	** e_{con}	c_{Dry} (g/cm ³)	q_{max} (kPa)
M-0%-020	9.61	0.379	0.378	1.952	301
M-0%-050	8.63	0.376	0.370	1.961	482
M-0%-100	9.66	0.417	0.405	1.938	804
M-0%-200	10.03	0.404	0.388	1.978	1177
M-0%-400	9.71	0.400	0.374	1.973	2067
M-1%-050	9.59	0.397	0.392	1.958	941
M-1%-100	8.44	0.367	0.357	1.974	1219
M-1%-200	8.72	0.392	0.364	1.968	1910
M-1%-300	9.83	0.410	0.381	1.943	2247
M-1%-400	9.03	0.393	0.350	1.965	2755
M-2%-020	9.21	0.380	0.380	1.961	809
M-2%-050	8.74	0.388	0.383	1.960	1359
M-2%-100	8.61	0.371	0.361	1.972	1656
M-2%-200	9.04	0.396	0.380	1.951	2157
M-2%-300	8.67	0.388	0.360	1.973	2718

* e_0 – initial void ratio.

** e_{con} is the void ratio after consolidation, before shearing.

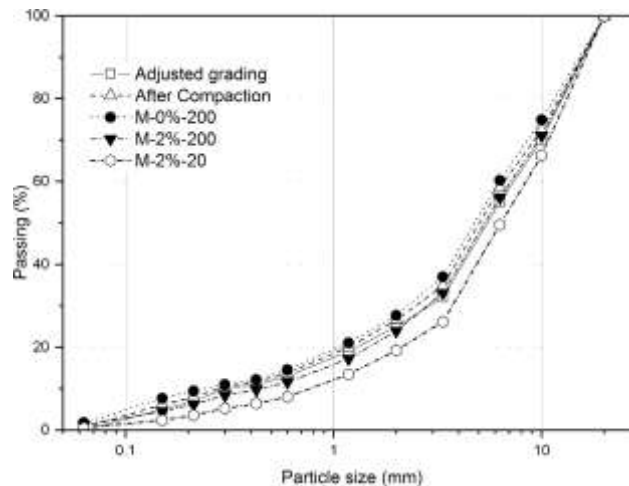


Fig. 3. Particle size distributions of the samples: original and after the compaction and monotonic shearing.

7. Therefore, the consolidation stage was extended even if the volume change wasnegligible.

During drained shearing a constant confining pressure was maintained throughout the test. The sample was sheared at a constant rate of strain of 0.016 mm/min, this was determined based on the capacity of the data acquisition system to interpret strains of 10^{-6} . Well after peak strength, the speed was doubled until the test was terminated. Tests were terminated either by achieving a constant strength and a constant volume, or by reaching an axial strain of 30%.

The moisture content was determined by using left over soil from the tray, and the initial void ratio of each sample was calculated in five different ways: an average of the initial dimensions, the volume of voids and solids, the dry unit weight and the final water content. Outliers were removed and an average of the values deemed acceptable was used. Although the samples were carefully prepared, a variation in the initial void ratio was unavoidable (Table 2).

4. Breakage

The idea of having a balance between particle breakage and particle rearrangement at critical state has been reported by many authors [(Chandler 1985, Daouadjiet al. 2001, Coop et al. 2004, Salim and Indraratna 2004, Muir Wood and Maeda 2008; Rubin and Einav 2011). The literature review has also shown that the level of breakage in dense granular materials, at lower pressures, is rarely investigated. It is often disregarded and assumed not to affect critical state, particularly when a large number of contacts is expected. Therefore, samples were sieved to evaluate breakage after shearing, whilst extra samples were prepared to determine if compaction caused particle breakage (Fig.3).

The results showed that after compaction small amounts of breakage can be seen in all sizes. Breakage was also seen after shearing, where the largest changes in PSD were seen in sizes ranging from 1 to 7 mm, where the increase in passing percentage is in the order of 8%. The smaller sizes have also increased, perhaps indicating the shearing of the asperities at the small confining stresses used.

An attempt to determine the PSD for the cemented samples was carried out by breaking the cement bonds before sieving, samples were put on individual sealed bags and the bonding destroyed by hand. Larger pieces that were kept intact were removed by hand, and only the soil that seemed not to have bonds was used. The results showed that the PSD curve of sample M 2%-200 is slightly above the original curve for sizes above 3 mm and below the original curve for sizes below 3 mm; whilst the M 2%-20 is below the original size tested (Fig. 3). This demonstrates

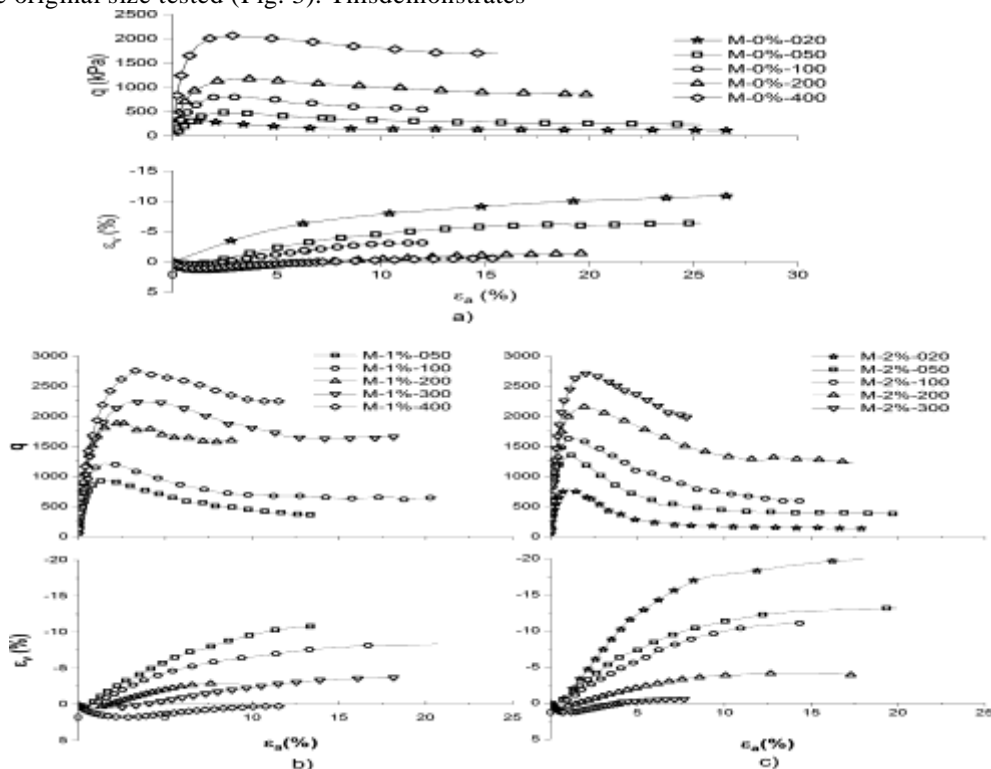


Fig. 4. Stress-strain and volumetric response of the soils tested with: a) 0%, b) 1% and c) 2% cement content.

the effect of the confining stress on the destruction of the bonds and the difficulty to destroy by hand, the bonds on the smallest sizes, even after a monotonic shearing has taken place.

5. Triaxial tests (stress-strainbehaviour)

The triaxial test results are shown on Fig. 4, where the stress-strain and the volumetric curves of 15 tests are plotted. As expected, all samples showed a strain-softening behaviour towards a constant strength after peak stress. The volumetric behaviour is similar; after a large dilation that reduces with the confining stress, it is possible to visualise a steady state, where no change in volume and strength is seen with the increase in shear strain. Large volumetric strains are also seen particularly at low stresses, where there are sharp changes in the volumetric behaviour, possibly indicating the occurrence of localisation. However, all samples have failed in barrelling and only in a few samples signs of localisation were noticed. A couple of tests were terminated earlier, due to small punctures on the membrane given the large strains. The axial strain, ϵ_a , was measured by two local displacement transducers up to a certain point (usually peak stress) switching to the external transducer afterwards.

The effect of the addition of cement in the strength is clear, as the peak values increase with the addition of cement for all confining stresses tested. Simultaneously, there is also an increase in the brittleness index (the ratio between the peak shear strength and the shear strength at large strains) of the samples. Fig. 5 shows the brittleness index calculated for all of the samples. The samples with 2% cement have a much larger brittleness index when compared to the other samples. It is also clear that the values of brittleness index calculated for the 1% cement samples have little deviation from the 0% samples; i.e., the addition of 1% cement causes small changes to this parameter.

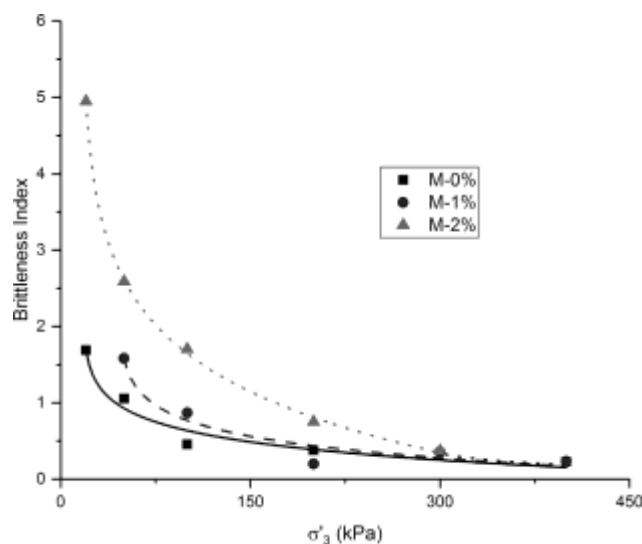


Fig. 5. The relationship between brittleness index and confining pressure.

The results also show that increasing the cement content reduces the level of strain required to reach the peak stress. This is true for every confining stress tested, confirming that there is an increase in stiffness with the addition of cement. Fig. 6 shows a direct comparison between the cemented and uncemented samples for certain confining stresses, to better show the effect of cementation in the peak shear strength and the volumetric behaviour, where higher cement content generates larger dilatative volumetric strains. For the uncemented soil, the area corresponding to the maximum rate of dilation directly corresponds to the peak strength, whilst the cemented samples experience peaks slightly before the maximum rate of dilation. The change seen is not large, but enough to demonstrate that small additions of cement can generate a structure that affects the strength of even very dense fabrics, as shown in Fig. 7. Fig. 8 shows the tangent stiffness curves (slope of the stress-strain curves) with arrows indicating the points where a change in shearing rate was performed to accelerate the tests. The gross yield points, regarded as the onset of bonding degradation and the locus where significant plastic deformations start to occur, are also indicated in the curves with the use of a black square. These were determined using the method proposed by Malandraki and Toll (1996) and Alvarado et al. (2012b) and are marked by the start of the change in direction of the stiffness curve. It is clear that the addition of cement increases the tangent stiffness; the tangent stiffness of the uncem-

entedsamplesstartatvalueslowerthan1GPa,whilstthesampleswith1%cementstartatvalueslowerthan2to3GPa, andthesampleswith2%showvalueslowerthan7or8GPa.Itcanalsobeseenthatincreasingthestrainreducesthetangent stiffness and that the rate of reduction in stiffnessisrelatedtothepercentageofcement(i.e.lowercementpercentages lower reductions and highercementpercentageshigher reductions). Comparing tests in each group, it is also seenthatincreasingtheconfiningpressurealsoresults in higherstiff nesses,despitethefactthatincertain samples this is not very clear and it is likely to be the effect of the scales used in the graph.

5.1. Stress-Dilatancy

A stress-dilatancy analysis was performed and Fig. 9 contains the plots of all 15 uncemented and cemented sam- ples, shown with the respective cement percentage. On each graph, the peak strength, the gross yield and last test point are represented by different symbols. The uncemented samples show an increase in the ratio q/p_0 with dilation, upto a peak, reached at the same time as the highest dilation rate. From that point onwards, dilation rate reduces together with the q/p_0 ratio. As the volume stops changing, a unique value of $M = 1.76$ can be determined, corresponding to a friction angle at critical state $u'_{cs} = 43^\circ$. The effect of the cement percentage can be seen by the initial change in the shape of the curve. At the start of shearing, as dilation develops, the samples quickly reach

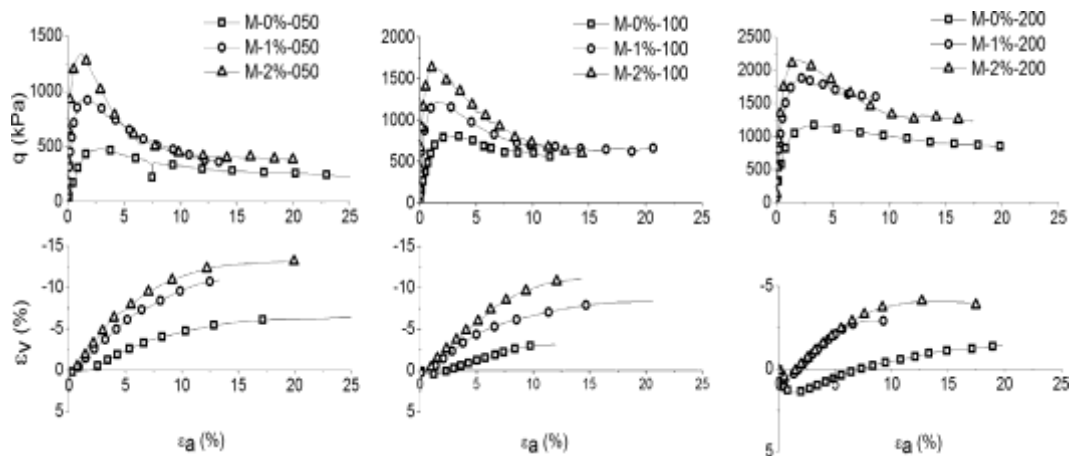


Fig. 6. Comparison of the stress-strain and volumetric responses of the samples with 0%, 1% and 2% cement, under different confining pressures.

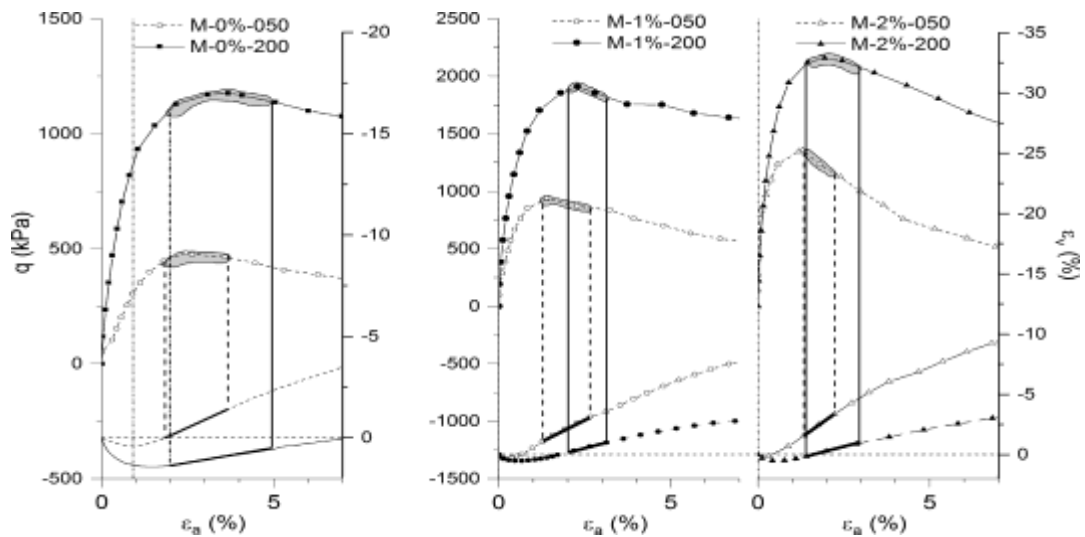


Fig. 7. Relationship between peak stress and maximum rate of dilation for 50 and 200 kPa confining stress: 0% cement on the left; 1% in the middle and 2% on the right.

high ratios of q/p^0 , indicating that the cementation is now active and allowing a stiffer response from the sample. This difference is proportional to the cement percentage; i.e., the higher cement percentage, the higher the ratio q/p^0 . The effects of cementation are also visible in the location of the peak stress, as it occurs before the maximum rate of dilation; this is similar to what was observed previously in Fig. 7 and described by Leroueil and Vaughan (1990). However, the difference between the ratio q/p^0 , measured at the peak stress and at the maximum rate of dilation is very small, indicating that the peak is largely governed by dilation rather than by cement content. The samples with 1% cement do not show this as clearly as the samples with 2% cement. Another expected behaviour is the reduction in dilation rate with the confining stress, seen in all cement and uncemented samples, similar to the behaviour of cemented sands, demonstrated by Coop and Willson (2003), Consoliel et al. (2012) and Alvarado et al. (2012b). The same authors have pointed out that after the maximum dilation rate the samples seem to follow a linear frictional trend, however, as the stress ratio reduces, the dilation rate seems to reduce much quicker, i.e. volumetric

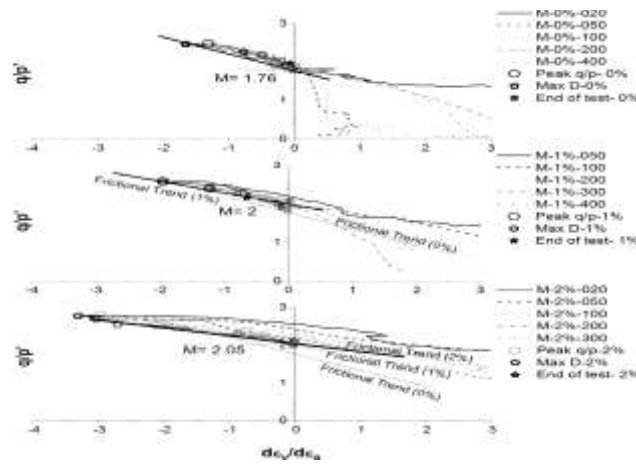


Fig. 8. Tangent stiffness against axial strain in log scale, together with the gross yield points for: (a) 0%, (b) 1% and (c) 2% cement.

strains change at a large rate, and the path moves inward and away from the frictional trend. The authors attribute this behaviour to the occurrence of localisation and the rapid reduction of volumetric strains. In the case of the sample tested here, a similar behaviour was observed after peak, however, as the shearing continues this trend is reversed and the samples seem to converge to a unique value of $M: M=2.00$ for 1% cement and $M=2.05$ for 2% cement. As can be seen in Fig. 9 and 9c, if the linear trend line is followed, a higher value of M is determined for the same percentages of cement, whilst in the case of Coop and Willson (2003), a lower value would be defined. The work done by Mühlhaus and Vardoulakis (1987) and Finno et al. (1997), show that the thickness of the shear band is proportional to the particle size distribution.

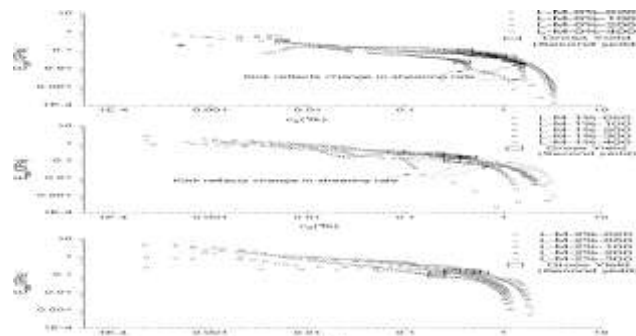


Fig. 9. Stress-dilatancy analysis: (a) 0%, (b) 1% and (c) 2% cement content.

Authors mention values of 16 and 10 to 25 times d_{50} respectively. Given that the triaxial sample has a finite volume this implies that the volumetric strains measured in a triaxial sample are a function of the grain size distribution. Therefore, variations in the grain size distribution during shear, will cause large changes in the dilation ratio. The samples tested are lightly cemented and the grain size distribution curve obtained after shearing, shows that the final grading has larger intermediate particles than the original grading. This indicates that there is an evolution of the particle size distribution during the shearing process. The DEM work done by Wang and Leung (2008a, 2008b), clearly shows that despite the shearing, there are still clusters of particles that remain intact within the sample. The authors, therefore, believe that as bonds degrade due to shearing there is a constant change in the particle size distribution. The consequence are seen as different volumetric strain rates that bring the dilation path inwards. As shearing continues, a more stable grading is achieved and a different value of M is reached at critical state.

6. Critical state

The points correspondent to the peak strength and the end of tests were plotted in Fig. 10, together with the results obtained from the Indirect Tensile tests (ITS) (BSEN13286-42:2003), as well as Unconfined Compressive tests (UCS) (BSEN 13286-41:2003), on samples of the same size, prepared using the same methodology. These samples are not shown on Table 2 but fall within the same

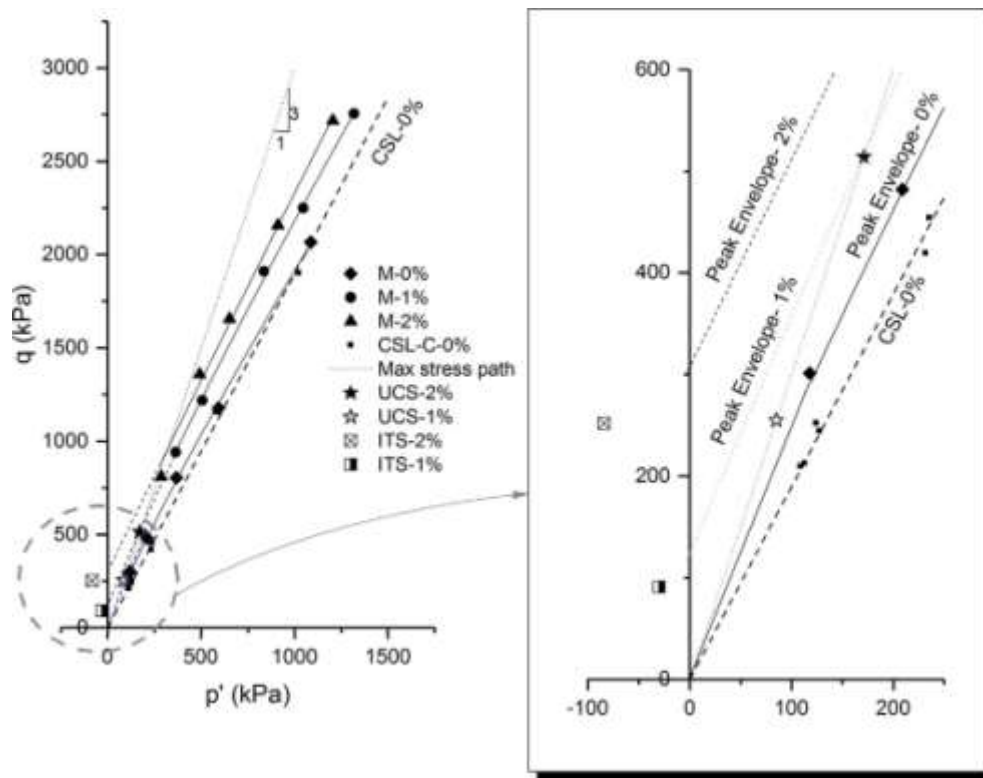


Fig. 10. Peak envelop on q versus p' diagram; the inset shows the small stresses region.

Table 3

Specification of peak and critical state line.

Type of crushed limestone	Critical state			Peak		
	C	M	$\angle_{cs} (^{\circ})$	q/p'	q Intercept	$\angle_p (^{\circ})$
Uncemented	0.053	1.747	1.77	1.81	0	46.6°
1% cement	0.101	2.054	2.00	1.90	265	45.9°
2% cement	0.122	2.218	2.05	2.03	299	46.7°

average values. These results served to plot the peak envelopes, as the cemented samples have a small tensile strength and it must be considered when defining the peak envelopes of the cemented soils. The failure envelopes plotted suggest values of M that are very similar to the values determined in the dilation plots above. Fig. 10b shows the small stress area with more detail. It is also important to point out that the peak envelope for the uncemented soil is curved and seems to join the CSL at p^0 of around 1100 kPa. The properties of the strength envelopes are shown on Table 3, where the peak friction angle for the uncemented soil was calculated assuming no cohesion.

Been et al. (1991) have shown that within the normal range of engineering stresses, sands show a steady state line at small stresses that is much shallower than at high stresses. Therefore, the paths followed by the tested samples were plotted on the specific volume, $\ln(p^0)$ space on Fig. 11, with the final point of each test indicated by a symbol. Although the arrows indicate the direction the tests were following when they were terminated, Fig. 4 shows that the magnitude of this movement was very small for most of the tests. The results show that there is no unique CSL for the cemented and uncemented soils. Instead, the results point clearly to the location of three distinct CSLs, one for each type of soil tested. The results also show that the addition of cement increases the slope of the CSL when compared to the uncemented soil. The larger dilative behaviour seen in the cemented samples is responsible for the steeper curve gradient shown by the cemented samples. A summary of the parameters obtained for the steady state lines in Fig. 11 is shown in Table 3.

The steady state lines determined for the cemented soils seem to reach a common point at stresses of around $p^0 = 1000$ kPa. This is compatible with the results shown by the grain size distribution curves, where the PSD of cemented samples sheared at large stresses is very similar to the PSD of the uncemented or original grain size distribution. As the percentages of cement content used in this

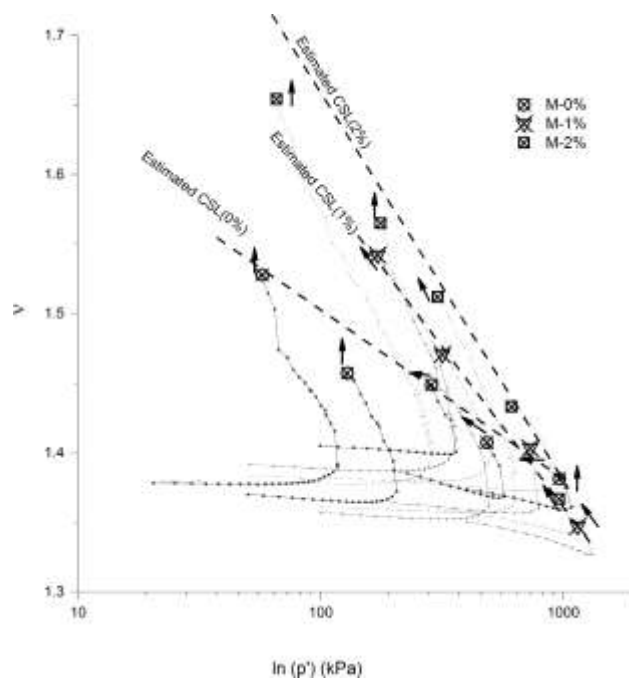


Fig. 11. Location of critical state lines for samples with 0%, 1% and 2% cement content on the specific volume, m , versus the logarithm of the mean effective stress, $\ln(p^0)$.

research were very small, the effect on the strength of the samples is likely to be felt only at small stresses. At larger confining stresses, the resultant frictional strength mobilised is much larger than the contribution of the cement. At that point the changes in the critical state lines caused by the cementation are very small.

6.1. Normalised behaviour

Given that the stresses used to consolidate the samples were very low and it was not possible to determine a Normal Compression Line (NCL), each set of tests was normalised with respect to M and the equivalent pressure on the CSL, by using Eq. (1) (k is the slope of the CSL, C is the specific volume at $p^0 = 1$ kPa and m is the specific volume, on the CSL and p'_{cs} is the mean effective stress on the CSL):

$$p_{cs}^0$$

$$\frac{1}{4} \exp \left(\frac{\Sigma}{C_m} \right)$$

The normalised stress paths show that it is possible to determine a state boundary surface for the peak states for each set of test up to the critical state line (broken line on Fig. 12). The normalised gross yield points determined from the stiffness curves for each set of tests was also plotted in Fig. 11. The gross yield envelopes are fully enclosed within the respective SBSs indicating that the cement percentages generated a very weak bonding. At low stresses, the yield surface seems to coincide with the SBS, however, as the stresses increase the yield surface moves inside and away from the SBS. The effect of the cement percentage

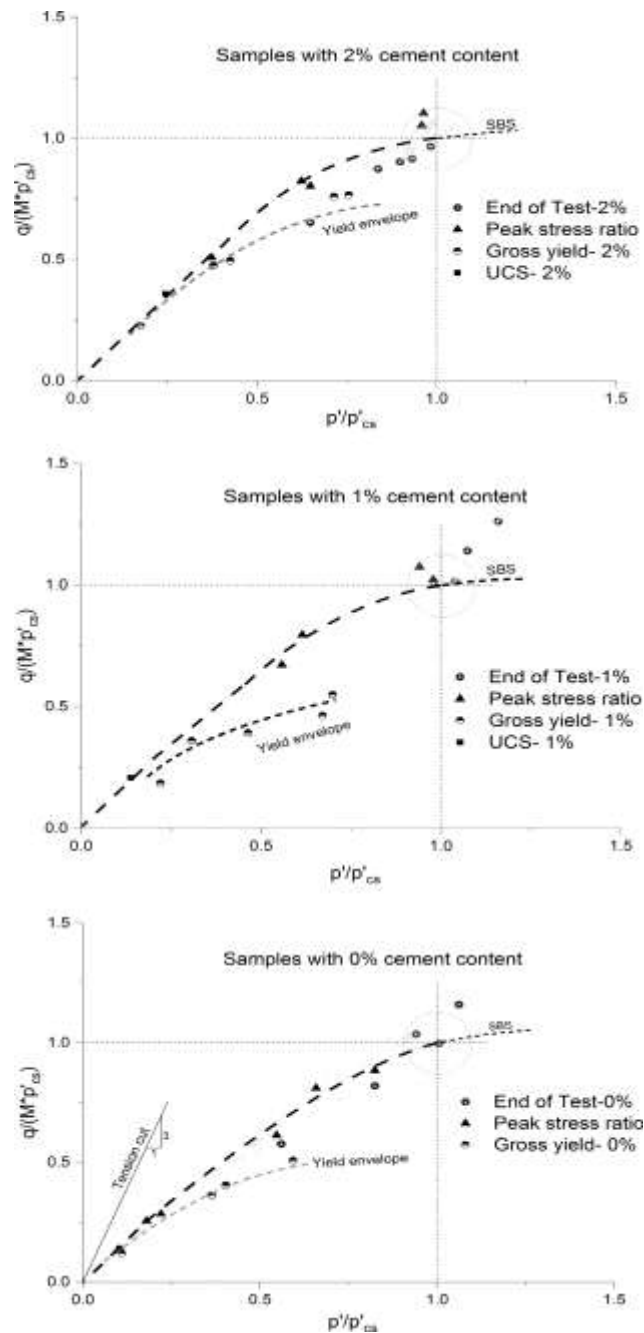


Fig. 12. Normalised yield and strength envelopes: (a) 0%, (b) 1% and (c) 2% cement.

is seen in the proximity between the gross yielding surface and the SBS, as the larger cement content keeps the yield surface closer to the SBS.

In Fig. 13 all the state boundaries and yield surfaces were plotted together. The results show that these are very

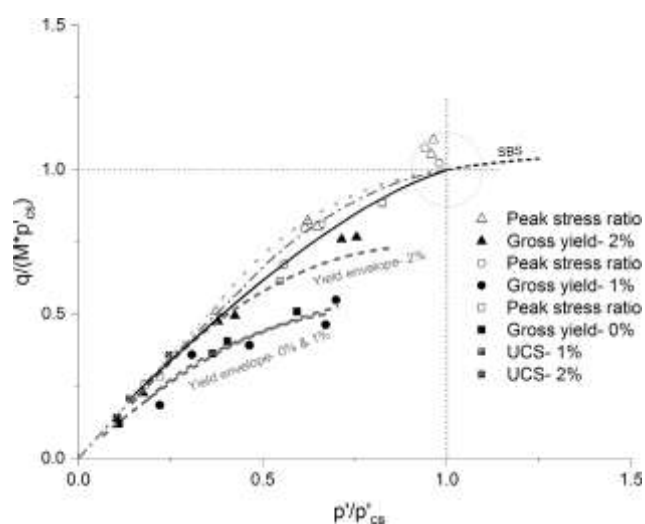


Fig. 13. Comparison of the normalized data for the uncemented and cemented soils.

similar, and a unique SBS could be used to represent the effect of the cemented and uncemented tests, when normalised by the CSL and the value of M . The gross yield surface of the uncemented and the 1% cement are coincident, however, a unique surface cannot be assumed as the 2% cement results have shown a significantly higher gross yield surface.

CONCLUSIONS

This work presents the findings of a study conducted in cemented and uncemented samples of a well graded compacted granular material, used for base and sub-base construction in the UK. The following conclusions can be drawn from this work:

- The mechanical properties of a well graded compacted granular material traditionally used in construction, can be further improved with the addition of small percentages of cement.
- The addition of cement also increases the dilatative tendency of these soils, providing better results particularly when small confining stresses are used as is the case of base and sub-base for road construction.
- The results show that it is possible to determine a unique Critical state line for the uncemented material and that the addition of cement will increase the slope of this line within the range of stresses commonly observed in engineering practice.
- When the data is normalised by the equivalent pressure on the CSL and the value of M , it is possible to determine a unique state boundary surface for the cemented and uncemented soils used in this research. The gross yield surface, however, is not unique and will depend on the cement percentage.

REFERENCES

- [1]. Alvarado, G., Coop, M.R., Willson, S., 2012a. On the role of bond breakage due to unloading in the behaviour of weak sandstones. *Géotechnique* 62(4), 303–316.
- [2]. Alvarado, G., Lui, N., Coop, M.R., 2012b. Effect of fabric on the behaviour of reservoir sandstones. *Can. Geotech. J.* 49(9), 1036–1051.
- [3]. Bandini, V., Coop, M.R., 2011. The influence of particle breakage on the location of the critical state line of sands. *Soils Found.* 51(4), 591–600.
- [4]. Been, K., Jefferies, M.G., Hachey, J., 1991. The critical state of sands. *Géotechnique* 41(3), 365–381.
- [5]. BS 1377-4: 1990. Soils for civil engineering purposes — Part 4: Compaction-related tests, London: British Standard Institute.
- [6]. BS EN 13286-41: 2003. Unbound and hydraulically bound mixtures. Test method for determination of the compressive strength of hydraulically bound mixtures. London: British Standard Institute.

- [7]. BS EN 13286-42: 2003. Unbound and hydraulically bound mixtures. Test method for the determination of the indirect tensile strength of hydraulically bound mixtures. London: British Standard Institute.
- [8]. BSEN1197-1:2011. Cement. Composition, specifications and conformity criteria for common cements. London: British Standard Institute.
- [9]. Carrera, A., Coop, M.R., Lancellotta, R., 2011. Influence of grading on the mechanical behaviour of Stava tailings. *Geotechnique* 61 (11), 935–946.
- [10]. 946.
- [11]. Chandler, H.W., 1985. A plasticity theory without drucker's postulate, suitable for granular materials. *J. Mech. Phys. Solids* 33 (3), 215–226.
- [12]. Coop, M.R., Atkinson, J.H., 1993. The mechanics of cemented carbonatesands. *Geotechnique* 43 (1), 53–67.
- [13]. Coop, M.R., Willson, S.M., 2003. Behavior of Hydrocarbon Reservoir Sands and Sandstones. *J. Geotech. Geoenviron. Eng.* 129 (11), 1010–1019.
- [14]. Coop, M.R., Sorensen, K.K., Freitas, T.B., Georgoutsos, G., 2004. Particle breakage during shearing of a carbonate sand. *Géotechnique* 54 (3), 157–163.
- [15]. Cuccovillo, T., Coop, M.R., 1997a. Yielding and pre-failure deformation of structured sands. *Géotechnique* 47(3), 491–508.
- [16]. Cuccovillo, T., Coop, M.R., 1997b. The measurement of local axial strains in triaxial tests using LVDTs. *Géotechnique* 47(1).
- [17]. Consoli, N.C., Dalla Rosa Johann, A., dos Santos, V.R., Corte, M.B., Moretto, R.L., Gauer, E.A., 2012. Key parameters for tensile and compressive strength of silt–lime mixtures. *Géotechnique Lett.* 2(May), 81–85.
- [18]. Consoli, N.C., Silva Lopes, L., Consoli, B.S., Festugato, L., 2014. Mohr Coulomb failure envelopes of lime-treated soils. *Geotechnique* 64 (2), 165–170.
- [19]. Cruz, N., Rodrigues, C., Viana da Fonseca, A., 2011. The influence of cementation in the critical state behaviour of artificial bonded soils. In: *International Symposium on Deformation Characteristics of Geomaterials*. pp. 730–737.
- [20]. Daouadji, A., Hicher, P.-Y., Rahma, A., 2001. An elastoplastic model for granular materials taking into account grain breakage. *Eur. J. Mech. A. Solids* 20 (1), 113–137.
- [21]. Delfosse-Ribay, E., Djeran-Maigre, I., Cabrillac, R., Gouvenot, D., 2004. Shear modulus and damping ratio of grouted sand. *Soil Dynam. Earthq. Eng.* 24 (6), 461–471.
- [22]. Finno, R.J., Harris, W.W., Mooney, M.A., Viggiani, G., 1997. Shear bands in plane strain compression of loess sand. *Géotechnique* 47(1), 149–165.
- [23]. Fuller, W.B., Thompson, S.E., 1907. The laws of proportioning concrete.
- [24]. *Trans. Am. Soc. Civil Eng.*, 59
- [25]. Ghafghazi, M., Shuttle, D.A., DeJong, J.T., 2014. Particle breakage and the critical state of sand. *Soils Found.* 54(3), 451–461.
- [26]. Haeri, S.M., Hamidi, A., Hosseini, S.M., Asghari, E., Toll, D.G., 2006. Effect of cement type on the mechanical behavior of a gravelly sand. *Geotech. Geol. Eng.* 24 (2), 335–360.
- [27]. Huang, J.T., Airey, D.W., 1993. Effects of cement and density on an artificially cemented sand. *Geotechnical Engineering of Hard Soils-Soft Rocks*. Balkema, Rotterdam, Athens, pp. 553–560.
- [28]. Kongsukprasert, L., Tatsuoka, F., 2007. Small strain stiffness and non-linear stress-strain behaviour of cemented-mixed gravelly soil. *Soils Found.* 47 (2), 375–394.
- [29]. Leroueil, S., Vaughan, P.R., 1990. The general and congruent effects of structure in natural soils and weak rocks. *Géotechnique* 40(3), 467–488.
- [30]. Lohani, T.N., Kongsukprasert, K., Watanabe, K., Tatsuoka, F., 2004. Strength and deformation properties of compacted cement-mixed gravel evaluated by triaxial compression test. *Soils Found.* 44(5), 95–108.
- [31]. Marri, A., Wanatowski, D., Yu, H.S., 2012. Drained behaviour of cemented sand in high pressure triaxial compression tests. *Geomech. Geoenviron. Eng.* 7 (3), 159–174.
- [32]. Malandraki, V., Toll, D.G., 1996. The definition of yield for bonded materials. *Geotech. Geol. Eng.* 14 (1), 67–82.
- [33]. Mühlhaus, H.B., Vardoulakis, I., 1987. The thickness of shear bands in granular materials. *Géotechnique* 37(3), 271–283.
- [34]. Muir Wood, D., Maeda, K., 2008. Changing grading of soil: effect on critical states. *Acta Geotech.* 3 (1), 3–14.
- [35]. Rios, S., Viana da Fonseca, A., Baudet, B., 2014. On the shearing behaviour of an artificially cemented soil. *Acta Geotech.* 9 (2), 215–226. <https://doi.org/10.1007/s11440-013-0242-7>.

- [36]. Rubin, M.B., Einav, I., 2011. A large deformation breakage model of granular materials including porosity and inelastic distortional deformation rate. *Int. J. Eng. Sci.* 49 (10), 1151–1169.
- [37]. Salim, W., Indraratna, B., 2004. A new elastoplastic constitutive model for coarse granular aggregates incorporating particle breakage. *Can. Geotech. J.* 41 (4), 657–671.
- [38]. Schnaid, F., Prietto, P.D.M., Consoli, N.C., 2001. Characterization of cemented sand in triaxial compression. *J. Geotech. Geoenviron. Eng.* 127 (10), 857–868.
- [39]. Shafabakhsh, G., Rezaeian, M., 2010. Analysis of the effects of applying different quantities and types of additives on strength parameters of cold in-situ recycled mixtures made of bitumen foam. *J. Transport. Res.* 7 (122), 53–66.
- [40]. Taheri, A.Y., Sasaki, Y., Tatsuoka, F., Watanabe, K., 2012. Strength and deformation characteristics of cemented-mixed gravelly soil in multi-step triaxial compression. *Soils Found.* 52 (1), 126–145.
- [41]. Tang, C., Shi, B., Gao, W., Chen, F., Cai, Y., 2007. Strength and mechanical behavior of short polypropylene fiber reinforced and cement stabilized clayey soil. *Geotext. Geomembr.* 25 (3), 194–202.
- [42]. Thevanayagam, S., Shenthan, T., Mohan, S., Liang, J., 2002. Undrained fragility of clean sands, silty sands, and sandy silts. *J. Geotech. Geoenviron. Eng.* 128 (10), 849–859.
- [43]. UK Highway Agency, 2016. Manual of contract documents for highway works volume 1 specification for highway works- road pavements — unbound, cement and other hydraulically bound mixtures (series 0800). Highway Agency. Available at: <http://www.standardsforhighways.co.uk/mchw/vol1/> (Accessed July 18, 2016).
- [44]. Wang, Y.-H., Leung, S.-C., 2008a. A particulate-scale investigation of cemented sand behavior. *Can. Geotech. J.* 45 (1), 29–44.
- [45]. Wang, Y.H., Leung, S.C., 2008b. Characterization of cemented sand by experimental and numerical investigations. *J. Geotech. Geoenviron. Eng.* 134 (7), 992–1004.
- [46]. Xiao, Y., Liu, H., Ding, X., Chen, Y., Jiang, J., Zhang, W., 2016. Influence of particle breakage on critical state line of rockfill material. *Int. J. Geomech.* 16 (1), 04015031.
- [47]. Yu, Y., Cheng, Y.P., Xu, X., Soga, K., 2014. DEM Study on the Mechanical Behaviours of Methane Hydrate Sediments: Hydrate Growth Patterns and Hydrate Bonding Strength. In: *Proceedings of the 8th International Conference on Gas Hydrates (ICGH8-2014)*. Beijing, China.
- [48]. Yu, Y., Cheng, Y.P., Xu, X., Soga, K., 2015. Shape effect of elongated soil particles on Discrete Element Modelling of methane hydrate soil sediments. *Geomech. Micro to Macro*, 207–212.